The Fine Structure of Intracranial Neoplasms Induced by the Inoculation of Avian Sarcoma Virus in Neonatal and Adult Rats

Dana D. Copeland, MD, Fred A. Talley, and Darell D. Bigner, MD, PhD

Groups of F-344 rats were inoculated with the Bratislava-77 strain of avian sarcoma virus (B-77-ASV) within 24 hours of birth, at 9 days of age, or between 97 and 119 days of age. Intracranial tumors developed in each age group. Multiple tumors with mixed histologic patterns developed in rats inoculated at 1 or 9 days of age. Solitary tumors with a uniform histologic pattern developed in rats inoculated as adults. On the basis of light and electron microscopic study, the majority of tumors in each age group were classified as astrocytomas and divided into either poorly differentiated, gemistocytic, pilocytic, or polymorphic varieties. The polymorphic astrocytomas were most common among neonatally inoculated rats, while the pilocytic astrocytomas were most common among rats inoculated as adults. Ultrastructural characteristics of astrocytes, including gap junctions and 7- to 9-nm filaments, were present in the majority of tumors in each age group. Astrocytomas induced in adult rats were remarkable for the presence of extensive basement membrane along the astrocytic cell surfaces. Intracytoplasmic virus-like particles (R particles) were common in the tumor cells. These virus-like particles are morphologically distinct from C-type B-77-ASV, and no morphologic evidence of C-type virus replication was observed in any of the tumors. (Am J Pathol 83:149–176, 1976)

INTRACEREBRAL INOCULATION of inbred F-344 rats with avian sarcoma virus (ASV) induces a high incidence of cerebral gliomas after short latency;[1,2] moreover, in rats, adult as well as neonatal animals have been shown to be susceptible to the neurooncogenic effects of cell-free ASV.[2] The induction of glial tumors in adult inbred rats provides a model for immunologic, transplantation, and therapeutic studies not feasible in randomly bred or neonatally inoculated animals.[2-4]

The majority of ASV-induced brain tumors in both neonatal and adult F-344 rats have been classified as astrocytomas by light microscopy; however, ultrastructural studies are critical for verification of glial characteristics in experimental brain tumors.[5-11] In the case of virally induced neoplasms as well as nonneoplastic disorders, ultrastructural studies are equally essential for the definition of virus–cell interaction; for example,

From the National Institute of Environmental Health Sciences, National Institutes of Health, Research Triangle Park, North Carolina, and the Department of Pathology, Duke University Medical Center, Durham, North Carolina.

Supported by Grants CA-14651 and CA-11895 from the National Cancer Institute. Dr. Bigner is the recipient of TIA Fellowship 1F11NS11063 from the National Institute of Neurological Disease and Stroke and a JFCF Award from the American Cancer Society.

Accepted for publication January 6, 1976.

Address reprint requests to Dr. Dana Copeland, National Institute of Environmental Health Sciences, Research Triangle Park, NC 27709.

in Burkitt's lymphoma,[12] subacute sclerosing panencephalitis,[13] and progressive multifocal leukoencephalopathy,[14,15] evidence implicating viral participation in the pathogenesis of the disease was first uncovered by electron microscopy. In the specific case of ASV, the replication of the defective Bryan strain in nonproducer cells was demonstrated by electron microscopy [16] after attempts to demonstrate viral replication by other means had failed.

For these reasons, we have undertaken a comparative study of brain tumors induced by the Bratislava-77 (B-77) strain of ASV by inoculation in both neonatal and adult F-344 rats. The presence of astrocytic ultrastructural features in the majority of tumors induced in both neonates and adults, the formation of basement membrane in the astrocytomas of the adult group, and the absence of morphologic evidence for replication of oncornavirus in these tumors is presented and discussed.

Material and Methods

Virus

Cell-free, homogeneous subgroup C, B-77-ASV was obtained, grown, concentrated, and titrated by previously described methods.[3]

Rats

Pregnant F-344 rats, CDF strain, were purchased from Charles River Laboratories, Wilmington, Mass. The size of the litters of these females was standardized to 8 pups per female. Experimental animals were drawn from these litters at ages calculated by counting the day of birth as the first postnatal day.

Inoculation

Rats were inoculated at three ages: within 24 hours of birth, at 9 days of age, and at 97 to 119 days of age. Virus was delivered in an inoculum of 0.005 ml (8.7×10^4 focus-forming units) in 0.05 M sodium citrate buffer pH 6.7. Neonates and 9-day-old rats were inoculated by previously described methods.[2] Adult rats (97 to 119 days old) were inoculated following methoxyflurane anesthesia, incision of the scalp, and perforation of the parietal bone posterior and lateral to the bregma with a 1 16-inch diameter bit in a hand-held electric drill. The viral inoculum was delivered through the perforation with a 1 4-inch 30-gauge needle, gastight microliter syringe, and automatic mechanical dispenser.

Fixation

Rats which developed symptoms of intracranial mass lesions were anesthetized with methoxyflurane and perfused through the left ventricle of the heart with buffered aldehydes at a perfusion pressure of 80 to 95 cm of water for 20 minutes. Four rats were perfused with a cacodylate-buffered solution of glutaraldehyde and paraformaldehyde initially at 20% aldehyde concentration and then at full strength.[17,18] The majority of symptomatic rats were perfused with a single strength phosphate-buffered 4% formaldehyde solution.[19]

Processing for Microscopy

Following perfusion, the brain was removed and divided by two midhorizontal slices 1 mm apart. Upper and lower portions were routinely processed and embedded whole in paraffin for light microscopy. Horizontal sections 8 μ thick were cut from these blocks and stained with hemotoxylin and eosin, phosphotungstic acid and hematoxylin, Holzer's technique, Gomori's reticulin technique, Van Gieson's method, Mellor's method, or Follis and Netsky's modification of Cajal's technique.[20,21] Rats found dead were autopsied, and brains fixed by immersion in phosphate-buffered formaldehyde [19] and processed as above for examination by light microscopy only.

The 1-mm-thick midhorizontal section was postfixed for 2 to 72 hours by immersion in fresh perfusate. Selected 1-mm blocks were then cut from this section and washed in 0.2 M sodium cacodylate buffer, postfixed in 1% osmium tetroxide for 2 hours, stained *en bloc* with 5% uranyl acetate,[22] dehydrated in graded ethanols, and embedded in Epon. Thick sections were cut at 1 μ and stained with toluidine blue for light microscopy. Silver to gold thin sections were cut on a Porter-Blum MT-1 microtome, mounted on uncoated copper grids, and examined at 80 kV in a Philips 300 electron microscope.

Results

A total of 146 rats were inoculated with B-77-ASV Of these, 47 were inoculated within 24 hours of birth. Each animal in this group of 47 developed at least one tumor, and most developed multiple neoplasms. One hundred and forty-five tumors were identified in this group, for a mean of 3.09 ± 1.23 tumors per animal inoculated. Mean survival among the rats inoculated on the first postnatal day was 83.8 ± 21.5 days with a range of 39 to 132 days (Table 1).

Thirty-seven rats were inoculated at 9 days of age. Fifty-six intracranial tumors were identified among these rats for a mean of 1.51 ± 0.84 tumors per animal inoculated. Just as in the group of rats inoculated on the first postnatal day, all rats inoculated at 9 days of age developed at least one intracranial tumor. Mean survival for the 9-day group was 166.1 ± 66.2 days, with a range of 54 to 323 days postinoculation.

Sixty-two rats were inoculated between 97 and 119 days of age; 325

Table 1—Tumor Incidence and Survival in F-344 Rats Inoculated With B-77-ASV

Age at inoculation (days)	Animals with tumors/animals inoculated	Tumors/animals inoculated	Mean tumors/ animal	Mean survival postinoculation (days)
1	47/47	145/47	3.09 ± 1.23	83.8 ± 21.5
9	37/37	56/37	1.51 ± 0.84	166.1 ± 66.2
97–119	37/62*	38/62*	0.61 ± 0.23*	183.0 ± 74.4*
Total	121/146	239/146	1.64 ± 1.37	139.3 ± 71.9

* Three hundred and twenty-five days after inoculation, 25 rats inoculated at 97 to 119 days of age were still surviving and free of symptoms of tumor.

days after inoculation. 25 of these rats were still surviving and free of neurologic symptoms. The 37 animals which had died or been killed after developing neurologic symptoms had a mean survival of 183.0 ± 74.4 days and a range of 74 to 309 days post inoculation. Each of 37 rats in this group which died or was killed had developed one intracranial tumor with the exception of 1 animal which developed two tumors. A total of 38 tumors among the rats inoculated as adults gives a mean of 0.61 ± 0.52 tumors per animal inoculated and a mean of 1.03 ± 0.23 tumors per moribund animal.

The tumors were classified on the basis of both light and electron microscopy. Preservation of ultrastructural detail by perfusion of phosphate-buffered formalin was judged to be equal to that achieved by perfusion of cacodylate-buffered mixed aldehydes. On the other hand, preparations of formaldehyde-fixed tissue were superior to paraformaldehyde-glutaraldehyde-fixed tissue for light microscopy. Comparison of blocks taken from formaldehyde-perfused brain and tumor after 2, 24, and 72 hours of immersion in fresh buffered formaldehyde and after 2 hours of postfixation in buffered formaldehyde, and 24 and 72 hours in sodium cacodylate buffer revealed no morphologic changes after prolonged immersion in either fixative or buffer. Thus blocks for examination by electron microscopy could be selected from the 1-mm midhorizontal slice after examination of an hematoxylin and eosin-stained horizontal section of adjacent brain by light microscopy. This technique greatly facilitated representative sampling of histologic patterns with a minimum number of blocks for examination by electron microscopy. A total of 28 tumors in 21 animals were studied by both light and electron microscopy. Ten of these tumors were in 5 rats inoculated within 24 hours of birth; 11 tumors were in 9 animals inoculated at 9 days of age; and 7 tumors were in 7 animals inoculated between 97 and 119 days of age.

Based on the results of both light and electron microscopy the tumors were divided into three broad categories: gliomas, sarcomas, and gliosarcomas. The glioma category was further subdivided into four subcategories: poorly differentiated astrocytoma, gemistocytic astrocytoma, pilocytic astrocytoma, and polymorphic astrocytoma. The distribution of tumors among these categories for each age group is shown in Table 2. A description of the histologic and ultrastructural features of each type follows.

Astrocytomas

The astrocytomas presented a variable morphologic picture in which three main cytologic types occurred in both homogeneous and mixed

Table 2—The Classification of B-77-ASV-Induced Neoplasms in F-344 Rats

Classification	Age at Inoculation								
	1 Day			9 Days			97-119 Days		
	No.	Total/ group	Percent/ group	No.	Total/ group	Percent/ group	No.	Total/ group	Percent/ group
Poorly differentiated astrocytoma	45			12			1		
Pilocytic astrocytoma	3			12			25		
Gemistocytic astrocytoma	21			0			0		
Polymorphic astrocytoma	47			9			6		
All astrocytomas	116	116/45	80%	33	35/56	59%	32	32/38	84.5%
Gliosarcomas	10	10/145	7%	7	7/56	13%	3	3/38	8%
Sarcomas	18	18/145	12%	14	14/56	25%	1	1/38	5%
Unclassified tumors	1	1/145	1%	2	2/56	4%	1	1/38	2.5%
Total	145	145/145	100%	56	56/56	100%	38	38/38	100%

patterns. Long, bipolar astrocytes, large round gemistocytic astrocytes, and small, poorly differentiated astrocytes could be found in most of the tumors. When one cell type clearly predominated, it was possible to assign the tumor to the corresponding astrocytic subcategory; when no cell type clearly predominated the tumor was designated a polymorphic astrocytoma.

Certain ultrastructural features were characteristic of all of the astrocytic cell types. Fine filaments 7 to 9 nm in diameter (Figure 18) were present in cytoplasm of all but the most poorly differentiated astrocytes (Figures 7 and 8) and were especially abundant in the long processes of the pilocytic astrocytes (Figure 18). End views of the filaments permitted visualization of a 2.5 to 4 nm hollow core (Figure 18). Gap junctions were present between astrocytes of each main category but were most common between the processes of pilocytic and poorly differentiated cells. A 2- to 3-nm gap between the outer leaflets of the apposed membranes was demonstrable (Figure 15).

Poorly Differentiated Astrocytoma

Tumors composed of dense sheets of small (4 to 8 μ) cells with high nuclear/cytoplasmic ratio, hyperchromatic oval nuclei, deeply basophilic cytoplasm, and frequent mitotic figures (Figure 3) were especially common in the periventricular region of rats inoculated at 1 or 9 days of age. By electron microscopy, these tumors were composed of a mixture of cell types forming a spectrum from very poorly differentiated forms with scant cytoplasm, few cytoplasmic organelles, and very short processes (Figure 7) to better differentiated forms with profiles of granular endoplasmic reticulum, an occasional Golgi apparatus, and a few glial filaments in moderately long processes which intertwined with the processes of adjacent cells (Figure 8). Nuclei of these cells were typically single, irregular in contour, with margination of nuclear chromatin and a central nucleolus (Figures 7 and 8).

Another component of the poorly differentiated tumors was a spongioblast-like cell. These bipolar cells had an oval nucleus and, typically, a single nucleolus. A few profiles of rough endoplasmic reticulum, mitochondria, and an occasional Golgi were characteristically present at one pole of the oval nucleus. Bundles of 7- to 9-nm filaments arose near the nucleus and continued into long processes which contained, in addition to the filaments, a few mitochrondria and free ribosomes (Figure 16). Junctions were common between both the poorly differentiated and spongioblast-like cells.

Gemistocytic Astrocytomas

Large, globoid cells with eosinophilic, hyaline, or foamy cytoplasm and one or more eccentrically placed nuclei (Figure 5) were present as a minor component in many of the neoplasms; however, only in rats inoculated at 1 day of age did cells of this type form discrete, homogeneous foci. Like the poorly differentiated astrocytomas, the gemistocytic astrocytomas were common in their periventricular regions of the lateral ventricles. Gemistocytic astrocytomas had a predilection for the hippocampus and periventricular region of the temporal horn of the lateral ventricles while poorly differentiated astrocytomas showed a predilection for the periventricular region of the basal ganglia. Although gemistocytic astrocytes predominated in none of the tumors in rats inoculated after 24 hours of age the distinctive large cells were present in multiple foci in many poorly differentiated, pilocytic and polymorphic tumors. Gemistocytic cells seemed to show a propensity for dispersion in cysts and throughout the subarachnoid space. In several different animals, gemistocytic astrocytes were observed to have invaded the stroma of the choroid plexus (Figure 13). Mitotic figures were not so common among the gemistocytic astrocytes as in the poorly differentiated tumors, but when present they were typically miltipolar and bizarre (Figure 5).

The fine structure of the gemistocytic forms was especially noteworthy for the richness and variety of cytoplasmic organelles and the characteristic appearance of the gemistocytic nucleus. The nucleus was always eccentrically placed. Chromatin was usually finely dispersed but on occasion was clumped just beneath the nuclear envelope. One or more nucleoli were typically present. Invaginations (Figure 11) of the nuclear membrane were common and in some cases so complex that it was impossible to judge if cells had multiple nuclei or just one extremely complex nucleus (Figure 12). In the center of the cell adjacent to the nucleus there was a rich assortment of cytoplasmic organelles including: mitochondria, rough endoplasmic reticulum, smooth endoplasmic reticulum, Golgi apparatuses, and lysosomes. Fine 7- to 9-nm filaments and rare 25-nm tubules were interlaced through the organelles of this region (Figure 10). Lipid droplets and cytosegresomes were also frequently present among the cytoplasmic organelles. In some cases the cytosegresomes were so intimately apposed to the lipid droplets that transition between the two seemed plausible (Figure 11). The periphery of the gemistocytic cells was not so rich in organelles as the center and most often contained only scattered free ribosomes in a matrix of glial filaments (Figure 10). Gemistocytes had only very short processes, and junctions between gemistocytes

were rare. In some regions, gemistocytic astrocytes were separated by a uniform 20- to 30-nm extracellular space, while in other areas the extracellular space was much larger and the cell surface of the gemistocytic cells was marked by numerous microvilli and pinocytotic vesicles (Figure 10). A basement membrane was present on the surface of the gemistocytic astrocytes only when juxtaposed to blood vessel walls (Figure 9).

No budding or extracellular C-type virus particles were observed in any of the tumors despite a thorough examination of more than 6,000 cells; however, a not uncommon feature of the gemistocytic astrocytes was the presence near the cisternae of the rough endoplasmic reticulum of clusters of 75- to 80-nm virus-like particles (Figure 10). These particles, which have been designated *R particles* and described in detail in a separate report,[23] consisted of a central core of 35 to 40 nm which was usually electron dense but occasionally had an electron-lucent center, a round peripheral shell about 7 to 8 nm thick, and spoke-like structures radiating between core and shell (Figure 10). In no case did the outer shell appear membranous even when the trilaminar structure of adjacent membranes was clearly resolved. R particles were not seen in the extracellular space or within the cisternae of the endoplasmic reticulum. While commonly seen in gemistocytic astrocytes, they were also found in pilocytic astrocytes and spongioblastic cells but were not seen in poorly differentiated cells.

Pilocytic Astrocytomas

The most common tumor type among the rats inoculated as adults was the pilocytic astrocytoma (Figures 4 and 6). These tumors were typically solitary and located in the region of the basal ganglia and cerebral cortex (Figure 1). Unlike the poorly differentiated astrocytomas, the pilocytic astrocytomas were only rarely contiguous with the subependymal zone. Serial sections confirmed that the tumors were entirely intraparencyhmal and were not contiguous with the meninges or the cranial nerves. By light microscopy this tumor was composed of intersecting streams of elongated spindle-shaped cells with oval nuclei. Mitoses were not uncommon but were not seen as frequently as in the poorly differentiated astrocytomas. Trabecular zones of necrosis were common in this tumor variety, and a dense network of reticulin in these necrotic areas around blood vessels and extending between tumor cells for some distance away from the blood vessel could be demonstrated by appropriate stains. Collagen deposition was confined to the vascular adventitia. The tumor cells were relatively uniform in appearance, but an occasional foci of gemistocytic forms was sometimes noted.

By electron microscopy the pilocytic astrocytes were remarkable for the

density of glial filaments in the long processes and for the frequent presence of basement membrane along the cell surface (Figures 17 and 18). In many sections, basement membrane could be traced from the perivascular region along the surfaces of the pilocytic processes. Away from the perivascular region, basement membrane was often discontinuous, and bundles of pilocytic cells and cell processes were covered by basement membrane only where the cell surface was exposed to a relatively large extracellular space (Figures 17 and 18). Collagen fibrils were present in the necrotic regions and around blood vessels but were not seen between tumor cells or cell processes.

The nucleus of the pilocytic cell was oval and frequently had a prominent nucleolus and finely dispersed chromatin. A few lamellae of rough endoplasmic reticulum and one or more Golgi complexes were present along with a few mitochondria in the perinuclear region. The overall appearance of the pilocytic astrocytes was similar to that of the spongioblast-like cells seen in the poorly differentiated astrocytoma with the exceptions that the nuclear/cytoplasmic ratio was higher in the spongioblast-like cells, glial filaments were more densely packed into the longer and more complex processes of the pilocytic cells, and the pilocytic cells had, in many cases, a basement membrane not seen in the spongioblast-like cells.

Polymorphic Astrocytomas

Many tumors especially among the rats inoculated on the first postnatal day were composed of a mosaic of the cell types described above. Within such tumors the transition from a region of one cell type to another might be abrupt (Figure 6) or more gradual. In other areas the different cell types were so mixed that it was impossible to identify a predominant cell type at all. Transitional forms intermediate between poorly differentiated and gemistocytic and poorly differentiated and pilocytic forms were common.

Gliosarcomas

Some neoplasms contained both mesenchymal and glial neoplastic elements. Such tumors typically had large foci of anaplastic mesenchymal cells with abundant reticulin and collagen deposition intermixed with gemistocytic or poorly differentiated astrocytic regions. Since mesenchymal proliferation in the leptomeninges and in the perivascular adventitia is associated with glial anaplasia, only those tumors in which mesenchymal elements were clearly anaplastic, invasive, and destructive of normal cytoarchitecture were assigned to the gliosarcoma category. The bound-

ary between mesenchymal and glial zones of these tumors was typically sharp and electron microscopy of blocks taken from these tumors revealed cell populations similar to either the sarcomas or the astrocytomas. Only rarely were fields seen in which mesenchymal and glial cells were mixed.

Sarcoma

Fibrosarcomas occurred intraparenchymally and in the meninges and in both cases most commonly in the posterior fossa. Grossly and microscopically the appearance of these tumors was similar to previously described ASV-induced intracranial sarcomas in rats,[1] hamsters,[5,7] and dogs.[6,9,10] The tumors were composed of sheets of spindle cells with pleomorphic, dense nuclei. Appropriate stains revealed a fine network of reticulin surrounding individual tumor cells throughout the neoplasm. Collagen deposition and calcification were common.

By electron microscopy, sarcomas consisted of irregularly shaped cells in a flocculent extracellular matrix interspersed with abundant collagen fibrils. Rough endoplasmic reticulin and multiple Golgi complexes were prominent in the cell cytoplasm. Fine filaments 5 to 7 nm in diameter were occasionally seen in small bundles just beneath the cell membrane but were not a prominent feature of the sarcoma cells. Nuclear chromatin was typically clumped beneath an irregular nuclear envelope. Cell junctions and basement membrane were not observed in the sarcomas.

Unclassified

Four tumors were not assigned to any of the above categories. In each case, tissue was available for light microscopy only. By light microscopic study, the tumors were tentatively diagnosed as: isomorphic oligodendroglioma (1), ependymoma (1), and hemangioma (2). In view of the rarity of tumors of these types among ASV-induced intracranial neoplasms and the unavailability of well-fixed tissue for electron microscopy, final classification of these tumors is withheld pending opportunity for fine structure study of similar ASV-induced neoplasms.

Discussion

The role of the subependymal cell plate in the genesis of tumors of the central nervous system has long been recognized.[24] The predilection of ASV-induced intracerebral neoplasms in the neonatally inoculated rat and dog for the subependymal zone is consistent with a postulated spread of viral inoculum throughout the ventricles in neonatally inoculated rats [2] and the subsequent transformation of cells in the subependymal zone.[25,26] Further supporting this hypothesis are the ultrastructural features des-

cribed in this study of the poorly differentiated astrocytomas which arise in this region.

The fine structure of the subependymal cells in many animals, including the rat, is well characterized.[27-30] Small cells with irregular nuclei and marginated chromatin, scant cytoplasm of medium electron density, many free ribosomes but little endoplasmic reticulum, few mitochondria and an occasional Golgi profile are common in the subependymal zone. These cells may be distinguished from microglia, lymphocytes, and macrophages by the absence of primary lysosomes in the subependymal cells.[27,31] Labeling studies with tritiated thymidine support the hypothesis that these poorly differentiated cells in the subependymal region may divide, migrate away from the ventricle into the cortex, and differentiate into astrocytes and oligodendrocytes.[32] Consistent with this observation, cells with fine structure intermediate between the subependymal cell and mature astrocytes have been described in the periphery of the subependymal zone. Such cells commonly have a few glial filaments in the cytoplasm and longer processes than the subependymal cells.[28] The similarities in fine structure between these poorly differentiated subependymal cells of the normal rat brain and the predominate cell type of the poorly differentiated B-77-ASV-induced astrocytomas, coupled with the tendency for tumors of this type to occur in the subependymal region of neonatally inoculated rats, support the hypothesis that such tumors arise by transformation of poorly differentiated glial precursors in this area. This hypothesis is consistent with experimental evidence in the dog in which electron microscopy of serial sections of the subependymal plate following intracerebral inoculation of ASV show ASV particles entering subependymal plate cells.[25,26]

Large round cells have been described in a number of both virally and chemically induced neoplasms in the rodent. The origin of such cells in ASV-induced mammalian tumors has been ambiguous since large cells with features of both gemistocytic astrocytes and vacuolated histocytes by light microscopy have been reported in both astrocytic and sarcomatous tumors.[33] Kumanishi[34] described large cells with eccentric nuclei, increased numbers of Golgi profiles, and 8-nm filaments in mouse brain tumors induced by inoculation of whole cell suspensions of Rous chicken sarcomas. Burger[5] described similar cells in ASV-induced intracerebral neoplasms in hamsters. Cells with similar morphology by light microscopy have been described in subcutaneously induced hamster sarcomas, in ASV-transformed chicken cell *in vitro*, and in ASV-induced primate brain tumors.[33] The large cells of the ASV-induced subcutaneous tumors very likely arise by transformation of mesenchymal cells. The large cells of the

ASV-induced brain tumors could arise by transformation of either neuroectodermal cells or mesenchymal elements associated with the vessels and coverings of the brain.

While the origin of such cells in ASV-induced brain tumor has been controversial, the neoplastic nature of similar large cells in rat brain tumors induced by ethyl-nitrosourea and methyl-nitrosourea has been questioned.[35,36] Lantos,[37] based on the ultrastructural study of ethyl-nitrosourea–induced brain tumors in BD-IX rats, has characterized such gemistocytic cells as reactive astrocytes.

The large gemistocytic astrocytes of the B-77-ASV–induced tumors in this study are clearly a proliferative component of the neoplasms. The presence of discrete homogeneous nodules of these cells in the rats inoculated within 24 hours of birth, the occurence of bizarre mitotic figures and extreme nuclear irregularity, and most importantly the invasion of choroid plexus and seeding of the subarachnoid space strongly support the anaplastic nature of these cells.

The astrocytic identity of the large cells is supported by the presence of 7- to 9-nm hollow filaments in the cytoplasm; occasional gap junctions, especially in cells intermediate in fine structure between the large gemistocytic cells and the poorly differentiated astrocytes; and the presence of a basement membrane over the surface of gemistocytic cells only when in apposition to the wall of a blood vessel.

Three morphologically distinct classes of intracellular filaments have been described in mammalian nervous tissue: 5-nm microfilaments, 6- to 9.5-nm glial filaments, and 9.5- to 13-nm neurofilaments.[38] Glial and neural filaments have a hollow core and a substructure consisting of 2.5- to 3.5-nm diameter globular subunits linked by fine crossbars.[39] Neurofilaments are reported to have an average external diameter of 11 nm and an average internal diameter of 3.5 nm, while glial filaments have an average external diameter of 7.5 nm and an average internal diameter of 2.5 nm.[39] The dimensions and substructure of the filaments in the ASV-induced tumors of this study are consistent with the dimensions of glial filaments.

Normal astrocytes are joined by both macula adherens and gap junctions in which appropriate tissue processing reveals a 2-nm gap between the outer leaflets of apposed astrocytes.[22] Such gap junctions have been observed in human gliomas [40] and human meningiomas;[41] experimental gliosis;[42] astrocytes responding to Wallerian degeneration;[43] B-77-ASV-induced astrocytomas in hamsters; and ependymal cells, neuronal processes, pial cells, and smooth muscle cells.[5] While neither gap junctions nor 7- to 9-nm hollow cytoplasmic filaments are specific astrocytic markers their joint occurrence in cells of an intraparenchymal brain tumor which

have a basement membrane only at the site of contact with blood vessels supports the astrocytic nature of the large round cells and the classification of tumors in which this cell type predominates as gemistocytic astrocytomas.

The classification of the pilocytic tumor is more problematic. The finding of extensive basement membrane formation was unexpected. The fine structural appearance of fusiform cells with basement membrane and long processes which interdigitate and sometimes form whorls is characteristic of the schwannoma. Furthermore, the light microscopic appearance of the pilocytic tumors would be consistent with a diagnosis of schwannoma, and intracerebral schwannomas of humans are reported in the literature.[44,45] On the other hand, intracerebral human tumors with a similar histologic pattern are usually classified as pilocytic astrocytomas or spongioblastomas. The similarity of the histologic patterns was underscored by Percival Bailey when he equated the terms *spongioblastoma* and *neuroma centrale* for the classification of intracerebral tumors of this type.[46]

Examination of serial sections of such tumors in adult rats of this study indicated that the tumors arose from a purely intracerebral site and were not contiguous with any of the cranial nerves at the base of the brain. Moreover, the intense glial fibrillogenesis, the presence of gap junctions, and the presence of cells intermediate in fine structure between the pilocytic forms and the poorly differentiated astrocytes support the astrocytic nature of these pilocytic cells. Basement membrane was often discontinuous and present only over the free surface of pilocytic cells not extending between closely apposed pilocytic processes, and collagen fibrils in the extracellular space of these tumors were extremely rare: these two features would be atypical for a schwannoma.

Under normal circumstances, astrocytes demonstrate a basement membrane over processes that are adjacent to vascular endothelium.[47,48] Recent work suggests that a variety of neuroepithelial cells—including embryonal retinal pigmented epithelium, developing neuroepithelium, and ethylnitrourea-induced rat astrocytoma cells *in vitro*—are capable of forming basement membrane and producing connective tissue proteins, including collagen.[49] Increased basement membrane production has also been noted in cultures of neoplastic astrocytes from human gliomas.[50]

For these reasons, we favor the diagnosis of pilocytic astrocytoma for these tumors and propose that the deposition of basement membrane along the surfaces of the pilocytic cells is either an alteration in the expression of the cell genome secondary to transformation or an augmentation in susceptibility to vectors which normally induce basement mem-

brane formation at the glial-mesenchymal interface so that in the ASV-induced tumors basement membrane is deposited along the astrocytic surface at a distance from the actual site of glial–mesenchymal contact.

Intracerebral inoculation of B-77-ASV in neonatal rats induces multiple poorly differentiated and gemistocytic astrocytomas in the periventricular region of the cerebral hemispheres while intracerebral inoculation of B-77-ASV in adult animals induces solitary pilocytic astrocytomas of the cerebral cortex and basal ganglia. Despite the differences in morphology and location between tumors in rats inoculated at different ages, the majority of B-77-ASV intracranial tumors at any age are astrocytomas with anaplastic cytologic and histologic features. While ASV-induced astrocytomas in the rat have many morphologic features in common with the most common human glioma, glioblastoma multiforme, there are significant morphologic differences, most notably the absence of endothelial proliferation in the rat tumors. The significance of these differences must be considered in perspective with the morphologic features of spontaneously occuring brain tumors in the rat. Spontaneous glioblastomas have been reported in the rat,[51-53] but the published photographs and descriptions of these tumors do not show or describe endothelial proliferation. Other large series of intracranial tumors in rats include no glioblastomas but show astrocytomas to be the most common intracranial tumor,[54,55] and describe considerable histologic variation including marked anaplasia within the astrocytoma category.[53] We suggest that strict application of the nosologic criteria developed for human tumors permits use of the term *glioblastoma multiforme* only when unequivocal endothelial proliferation is present; thus, true spontaneous glioblastomas, if they occur in rats at all, must be exceedingly rare. The most common type of spontaneous rat brain tumor is the anaplastic astrocytoma and in this respect B-77-ASV–induced intracranial tumors in the rat, especially those induced by inoculation of adult animals, parallel spontaneously occurring intracranial tumors of the rat and represent a pathologic abberation from the normal in the rat that is homologous to the aberration represented by glioblastoma multiforme in the human.

Virus-like particles have occasionally been reported in ultrastructural studies of human brain tumors, but none of the morphologic observations have been confirmed and some reports have been shown to be spurious observations of nonviral cellular components.[33] Negative morphologic findings in the case of C-type oncornaviruses are especially significant since budding of the virus through the cell membrane is a characteristic and necessary feature of oncornavirus replication. While viruses may play a role in the induction of human brain tumors, it seems unlikely that

human tumors grow by replication of complete virus which is then released into the extracellular space and then infects and transforms neighboring cells. The absence of morphologic evidence of viral replication and budding into the extracellular space is, therefore, an important criteria in the selection of an animal model for human brain tumors.

C-type virus particles in mammalian ASV–induced brain tumors have been detected only once in an ultrastructural study of a canine meningeal tumor.[6] Mammalian cells are typically nonpermissive for ASV replication; however, B-77-ASV may rarely transform and replicate fully infectious virus in rat cells.[56] In the present study, no extracellular C-type particles or evidence of virus budding was seen in any of the over 6,000 cells in the 28 tumors studied by electron microscopy. In another series of B-77-ASV–induced rat brain tumors, no infectious virus was detected by biologic assay.[4] Although virus replication could occur at levels so low as to escape detection, the absence of either morphologic or biologic evidence of B-77-ASV replication suggests rat B-77-ASV–induced tumors do not grow primarily through infection and transformation of neighboring cells with fully replicated B-77-ASV.

Intracytoplasmic virus-like particles, R particles, were seen in many tumor cells, but we believe these particles are unrelated to B-77-ASV. R-type virus-like particles have previously been observed in BHK-21 hamster cell lines, in virus-transformed BHK-21 cells, in chemically induced hamster tumors, and in B-77-ASV–induced rat brain tumors,[23] but biologic activity of the R-particles has not been demonstrated.[23] Unlike the intracytoplasmic location of the R particles in the rat cells in this study, most of the R particles in hamster cells have been seen in the intracisternal spaces. Intracisternal R particles in hamster cells are typically membrane bound, and budding through the membranes of the endoplasmic reticulum has been reported; acquisition of the outer envelope from the intracellular cisternal membranes is, therefore, likely.

The viral inoculum used to induce the tumors studied in this report and the inoculum used in the original report of R particles in B-77-ASV-induced brain tumors came from a common viral pool which was, in turn, grown from virus rescued from hamster glioma cells which had been induced by uncloned B-77-ASV. Although no virus particles were seen in the hamster gliomas and no R particles detected by electron microscopy of viral pellets from the inoculating pool of B-77-ASV, the R particles may have originated from the rescue of an endogenous hamster viral genome from the hamster glioma cells.[23] Failure to bud through the cisternal membrane in rat cells would account for the absence of an outer envelope and for the extracisternal, intracytoplasmic distribution of the R particles

in the neoplastic rat cells. The biologic activity and role of R particles can only be fully assessed following their isolation and further characterization.

References

1. Wilfong RF, Bigner DD, Self DJ: Brain tumor types induced by the Schmidt-Ruppin strain of Rous sarcoma virus in inbred Fischer rats. Acta Neuropathol 25:196–206, 1973
2. Copeland DD, Vogel FS, Bigner DD: The induction of intracranial neoplasms by the inoculation of avian sarcoma virus in perinatal and adult rats. J Neuropathol Exp Neurol 34:340–358, 1975
3. Bigner DD, Self DJ, Frey J, Ishizaki R, Langlois AJ, Swenberg JA: Refinement of the avian oncornavirus-induced primary rat brain tumor model for therapeutic screening. Current Concepts in Cancer Research. Edited by T Hekmatpanah. New York, Springer-Verlag, 1975, pp 20–34
4. Bigner DD, Pegram CN, Vick NA, Copeland DD, Swenberg JA: Characterization of the avian sarcoma virus induced mammalian brain tumor model for immunological and chemotherapeutic studies. Proceedings of the Seventh International Congress on Neuropathology, Budapest. Amsterdam, Excerpta Medica, 1975, pp 445–450
5. Burger PC, Bigner DD, Self DJ: Morphologic observations of brain tumors in PD4 hamsters induced by four strains of avian sarcoma virus. Acta Neuropathol 26:1–21, 1973
6. Bucciarelli E, Rabotti GF, Dalton AJ: Ultrastructure of meningeal tumors induced in dogs with Rous sarcoma virus. J Natl Cancer Inst 38:359–381, 1967
7. Bucciarelli E, Rabotti GF, Dalton AJ: Ultrastructure of gliomas induced in hamsters with Rous sarcoma virus. J Natl Cancer Inst 38:865–889, 1967
8. Haguenau F, Rabotti GF, Lyon G, Moraillon A: Gliomas induced by Rous sarcoma virus in the dog: An ultrastructural study. J Natl Cancer Inst 46:539–559, 1971
9. Haguenau F, Rabotti GF, Lyon G, Moraillon A: Tumeurs cérébrales experimentales d'étiologie viral chez le chien. Rev Neurol (Paris) 126:347–370, 1972
10. Vick NA, Bigner DD, Kvedar JP: The fine structure of canine gliomas and intracranial sarcomas induced by the Schmidt-Ruppin strain of the Rous sarcoma virus. J Neuropathol Exp Neurol 30:354–367, 1971
11. Vick NA, Bigner DD: Some structural aspects of dog brain tumors induced with the Schmidt-Ruppin strain of the Rous sarcoma virus. Prog Exp Tumor Res 17:59–73, 1972
12. Epstein MA, Achong BG, Barr VM: Virus particles in cultured lymphoblasts from Burkitt's lymphoma. Lancet 1:702–703, 1964
13. Bouteille M, Fonaine C, Vedrenne C, Delarue J: Sur un cas d'encephalite subaigue à inclusions: Etude anatamo-clinique et ultrastructurale. Rev Neurol (Paris) 113:454–458, 1965
14. Silverman L, Rubinstein LJ: Electron microscopic observations on a case of progressive multifocal leukoencephalopathy. Acta Neuropathol 5:215–224, 1965
15. ZuRhein GM, Chou SM: Particles resembling papova viruses in human cerebral demyelinating disease. Science 148:1477–1479, 1965
16. Dougherty RM, DiStefano HS: Virus particles associated with "nonproducer" Rous sarcoma cells. Virology 27:351–359, 1965
17. Karnovsky MJ: A formaldehyde-glutaraldehyde fixative of high osmolality for use in electron microscopy. J Cell Biol 27:137A, 1965
18. Reese TS, Karnovsky MJ: Fine structural localization of a blood-brain barrier to exogenous peroxidase. J Cell Biol 35:213–236, 1967

19. Carson FL, Martin JH, Lynn JA: Formalin fixation for electron microscopy: A re-evaluation. Am J Clin Pathol 59:365–373, 1973
20. Luna LG: Manual of Histological Staining Methods of the Armed Forces Institute of Pathology, Third edition. New York, McGraw-Hill Book Co., 1968
21. Folliss AGH, Netsky MG: Astrocytes in formalin-fixed paraffin sections. Tech Bull Regist Med Technol 39:416–419, 1969
22. Brightman MW, Reese TS: Junctions between intimately apposed cell membranes in the vertebrate brain. J Cell Biol 40:648–677, 1969
23. Cloyd MW, Burger PC, Bigner DD: R-type virus-like particles in avian sarcoma virus-induced rat cerebral nervous system tumors. J Natl Cancer Inst 54:1479–1482, 1975
24. Globus JH, Kuhlenbeck H: The subependymal cell plate (matrix) and its relationship to brain tumors of the ependymal type. J Neuropathol Exp Neurol 3:1–35, 1944
25. Vick NA, Bigner DD; Early and sequential structural events in the neoplastic transformation of glia by the Rous sarcoma virus.[4] pp 437–444
26. Vick NA, Bigner DD: Gliomas induced by avian sarcoma virus (ASV): Early and sequential structural events of the neoplastic transformation in vivo. J Neuropathol Exp Neurol 34:99, 1975
27. Blakemore WF: The ultrastructure of the subependymal plate in the rat. J Anat 104:423–433, 1969
28. Caley DW, Maxwell DS: An electron microscopic study of the neuroglia during postnatal development of the rat cerebrum. J Comp Neurol 133:45–70, 1968
29. Privat A, Leblond CP: The subependymal layer and neighboring region in the brain of the young rat. J Comp Neurol 146:277–302, 1972
30. Ling EA, Paterson JA, Privat A, Mori S, Leblond CP: Investigation of glial cells in semithin sections. I. Identification of glial cells in the brain of young rats. J Comp Neurol 149:43–72, 1973
31. Mori S, Leblond CP: Identification of microglia in light and electron microscopy. J Comp Neurol 135:57–80, 1969
32. Paterson JA, Privat A, Long EA, Leblond CP: Investigation of glial cells in semithin sections. III. Transformation of subependymal cells into glial cells, as shown by radioautography after ^{3}H-thymidine injection into the lateral ventricle of the brain of young rats. J Comp Neurol 149:83–102, 1973
33. Bigner DD, Pegram CN: A review of virus-induced experimental brain tumors and of the putative associations of viruses with human brain tumors. Adv Neurol 13:57–83, 1976
34. Kumanishi T, Ikuta F, Yamamoto T: Brain tumors induced by Rous sarcoma virus, Schmidt-Ruppin strain. III. Morphology of brain tumors induced in adult mice. J Natl Cancer Inst 50:95–109, 1973
35. Lantos PL: The fine structure of periventricular pleomorphic gliomas induced transplacentally by *N*-ethyl-*N*-nitrosourea in BD-IX rats with a note on their origin. J Neurol Sci 17:443–460, 1972
36. Swenberg JA, Koestner A, Wechsler W: The induction of tumors on the nervous system with intravenous methylnitrosourea. Lab Invest 26:74–85, 1972
37. Lantos PL: An electron microscope study of reacting astrocytes in gliomas induced by *N*-ethyl-*N*-nitrosourea in rats. Acta Neuropathol 30:175–181, 1974
38. Johnson LS, Sinex FM: On the relationship of brain filaments to microtubules. J Neurochem 22:321–326, 1974
39. Wuerker RB: Neurofilaments and glial filaments. Tiss Cell 2:1–9, 1970
40. Tani E, Nishiura M, Higashi N: Freeze-fracture studies of gap junctions of normal and neoplastic astrocytes. Acta Neuropathol 26:127–138, 1973
41. Tani E, Ikeda K, Yamagata S, Nishiura M, Higashi N: Specialized junctional complexes in human meningioma. Acta Neuropathol 28:305–315, 1974

42. Tani E, Ametani T: Intercellular contacts of human gliomas. Progress in Neuropathology, Vol I, Edited by HM Zimmerman. New York, Grune and Stratton, 1971
43. Vaughan JE, Pease DC: Electron microscopic studies of Wallerian degeneration in rat optic nerves. J Comp Neurol 140:207–226, 1970
44. Ghatak NR, Norwood C, Davis CH: Intracerebral schwannoma. Surg Neurol 3:45–47, 1975
45. Gibson AA, Hendrick EB, Conen PE: Intracerebral schwonnoma: Report of a case. J Neurosurg 24:552–557, 1966
46. Bailey P: Cellular types in primary tumors of the brain. Cytologic and Cellular Pathology of the Nervous System. Edited by W Penfield. New York, Hafner, 1932, p 917
47. Caley DW, Maxwell DS: Development of the blood vessels and extracellular spaces during postnatal maturation of rat cerebral cortex. J Comp Neurol 138:31–47, 1970
48. Peters A, Palay SL, Webster HD: The cells and their processes. The Fine Structure of the Nervous System. New York, Harper & Row, 1970
49. Sipe JC, Rubinstein LJ, Herman MM, Bignami A: Ethylnitrosourea-induced astrocytomas: morphologic observations on rat tumors maintained in tissue and organ culture systems. Lab Invest 31:571–579, 1974
50. Sipe JC, Herman MM, Rubinstein LJ: Electron microscopic observations on human glioblastomas and astrocytomas maintained in organ culture systems. Am J Pathol 73:589–606, 1973
51. Mawdesley-Thomas LE, Newman AJ: Some observations on spontaneously occuring tumors of the central nervous system of Sprague-Dawley rats. J Pathol 112:107–116, 1974
52. Newman AJ, Mawdesley-Thomas LE: Spontaneous tumors of the central nervous system of laboratory rats. J Comp Pathol 84:39–50, 1974
53. Saxton JA, Spering GA, Barnes CC, McCay CM: The influence of nutrition upon the indicence of spontaneous tumor of the albino rat. Acta Unio Int Contra Cancrum 6:423–431, 1948.
54. Fitzgerald JE, Schardein JL, Kurtz SM: Spontaneous tumors of the nervous system in albino rats. J Natl Cancer Inst 52:265–273, 1974
55. MacKenzie WF, Garner FM: Comparison of neoplasms in six sources of rats. J Natl Cancer Inst 50:1243–1257, 1973
56. Altaner C, Svec F: Virus production in rat tumors induced by chicken sarcoma virus. J Natl Cancer Inst 37:745–752, 1966

Acknowledgments

We thank Pat Parker, Phylis Merritt, and Bernard Lloyd for their skill in the processing of tissue for microscopy; Carl Bishop, Bill Boyarksy, and Jessie Calder for the preparation of the micrographs; Linda Brogan for the typing of the manuscript; and Drs. Peter Burger, John Shelburne, and F. Stephen Vogel for review of the manuscript and valuable suggestions.

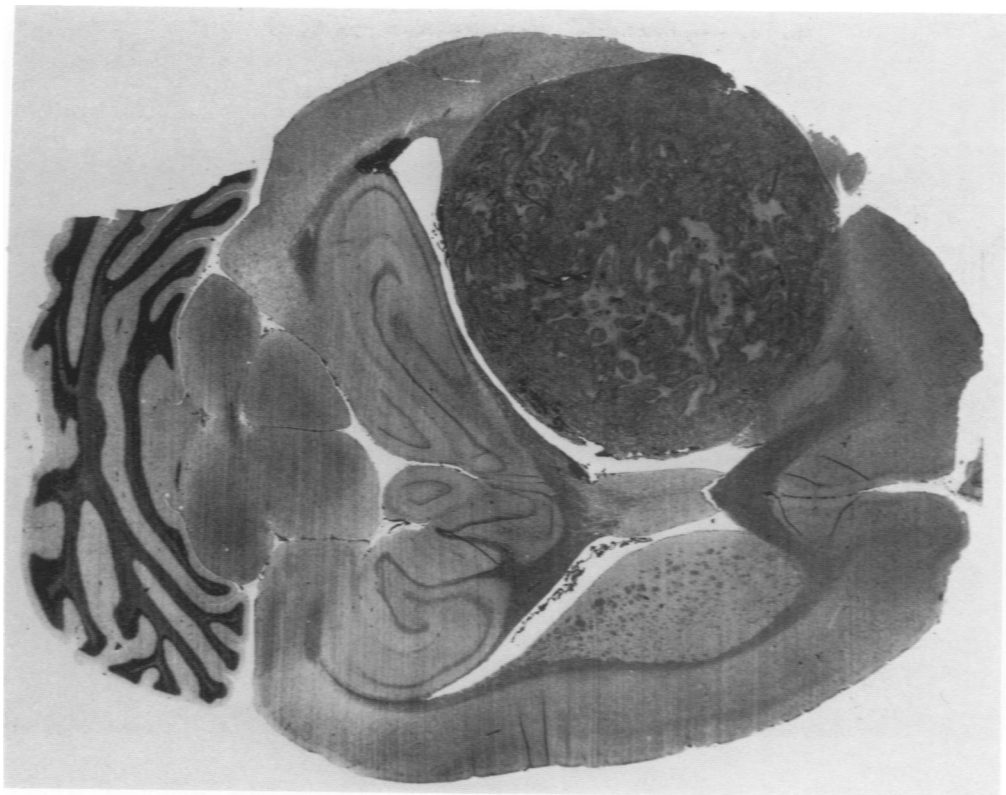

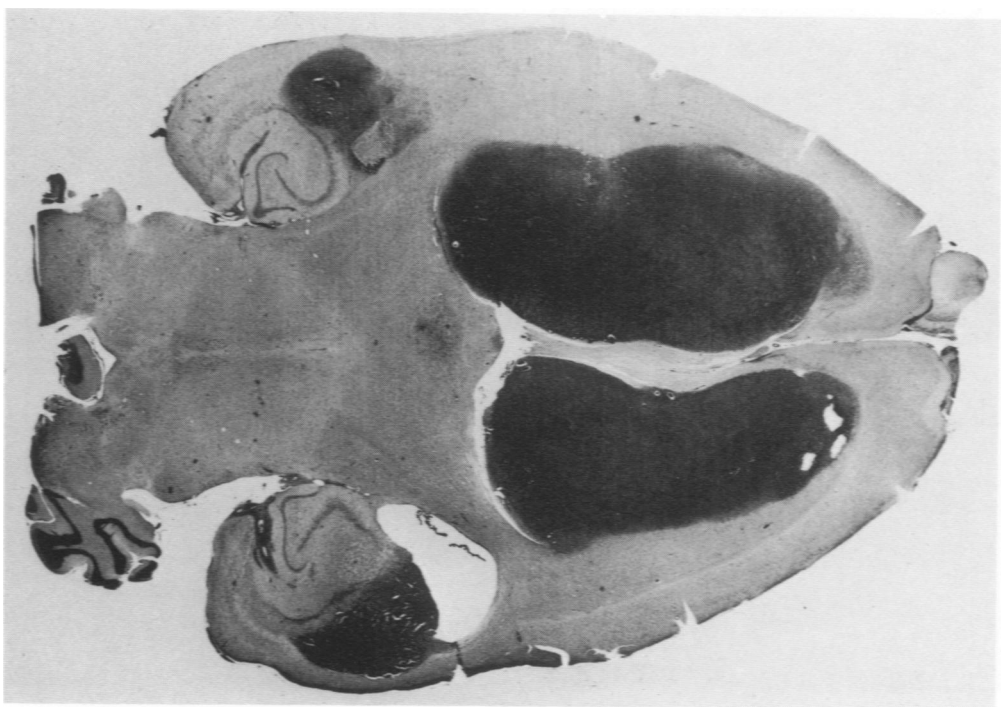

Figure 1—Horizontal section of brain from rat inoculated with B-77-ASV at 97 days of age. Solitary cerebral tumor with pale necrotic zones. (H&E, × 6.4) **Figure 2**—Horizontal section of brain from rat inoculated with B-77-ASV within 24 hours of birth. Bilateral tumors of basal ganglia and temporal lobes. (H&E, × 6.4)

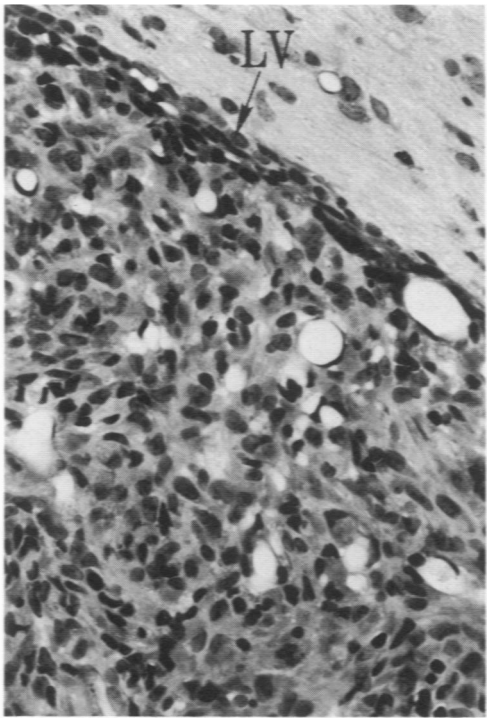

3

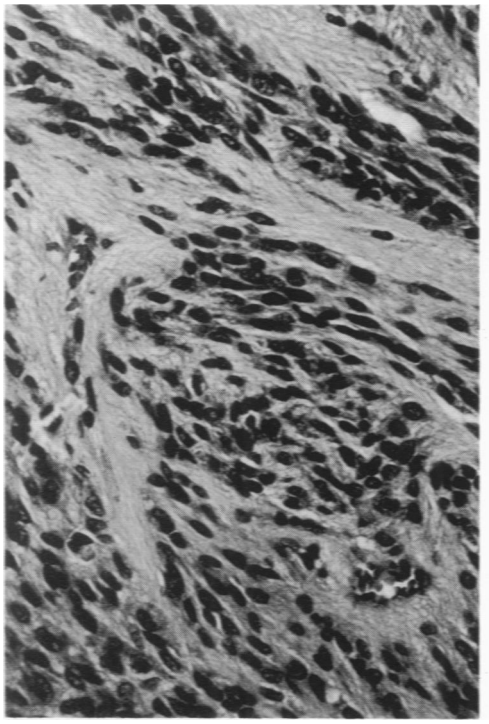

4

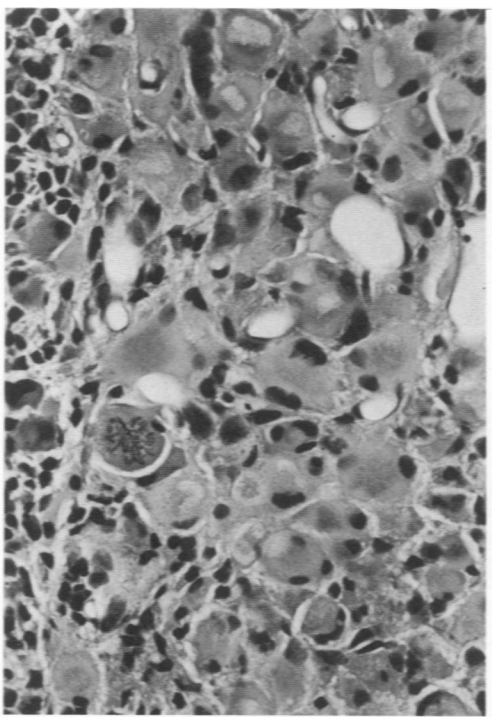

5

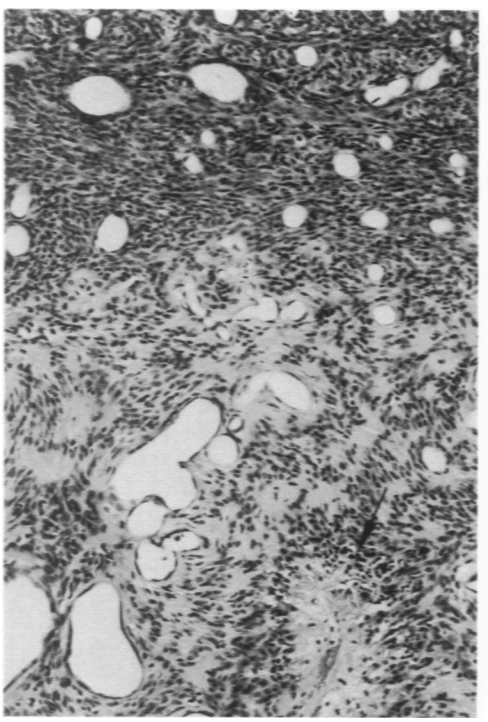

6

Figure 3—Poorly differentiated astrocytoma beneath ependyma of collapsed lateral ventricle (*LV*) (H&E, × 275). **Figure 4**—Pilocytic astrocytoma (H&E, × 275). **Figure 5**—Gemistocytic astrocytoma (H&E, × 275). **Figure 6**—Transition between poorly differentiated astrocytoma at top and pilocytic astrocytoma at bottom. Note necrosis and pseudopallisading of nuclei (*arrows*). (H&E, × 100)

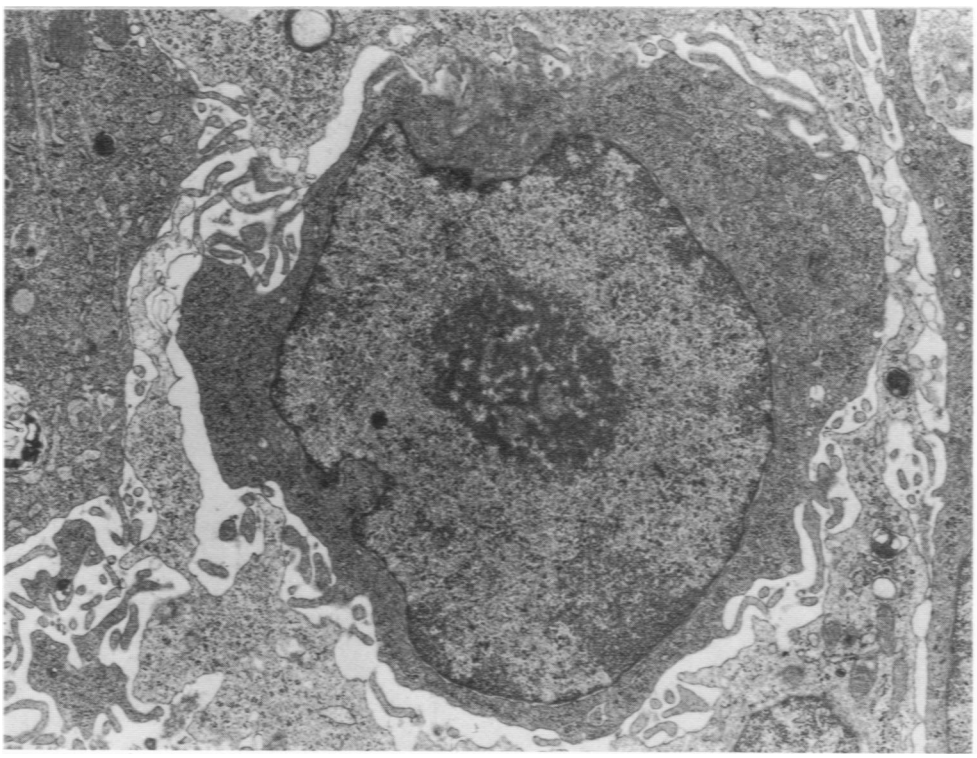

7

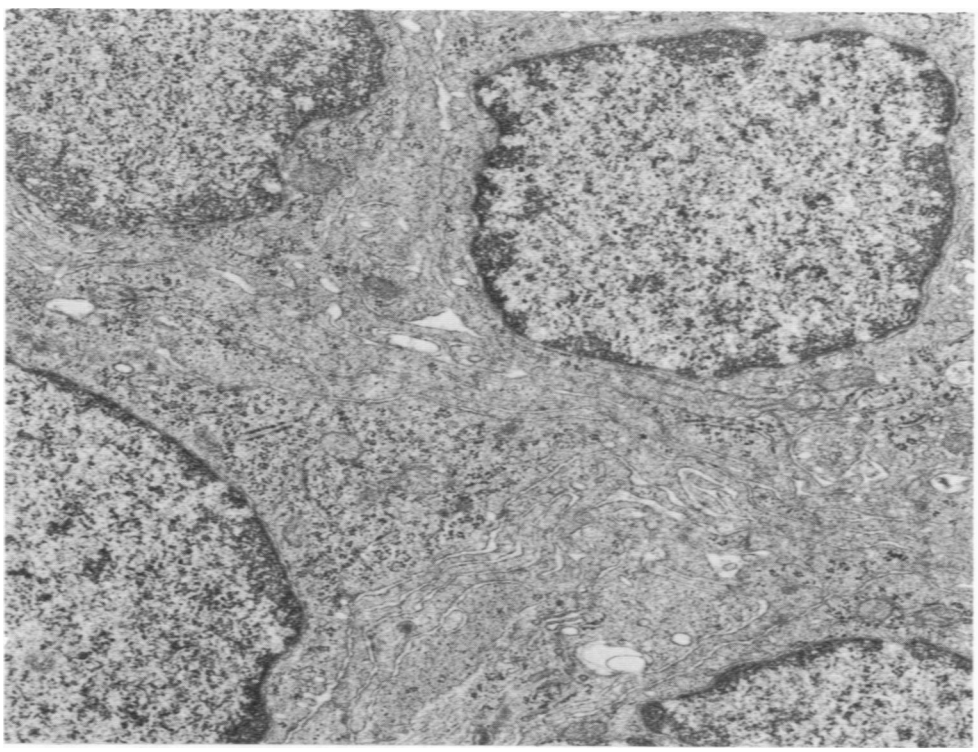

8

Figure 7—Poorly differentiated cell in a subependymal tumor of a neonatally inoculated rat (Formaldehyde fixation, × 10,620). **Figure 8**—Moderately well-differentiated astrocytes in a subependymal tumor of a neonatally inoculated rat (Glutaraldehyde fixation, × 18,780)

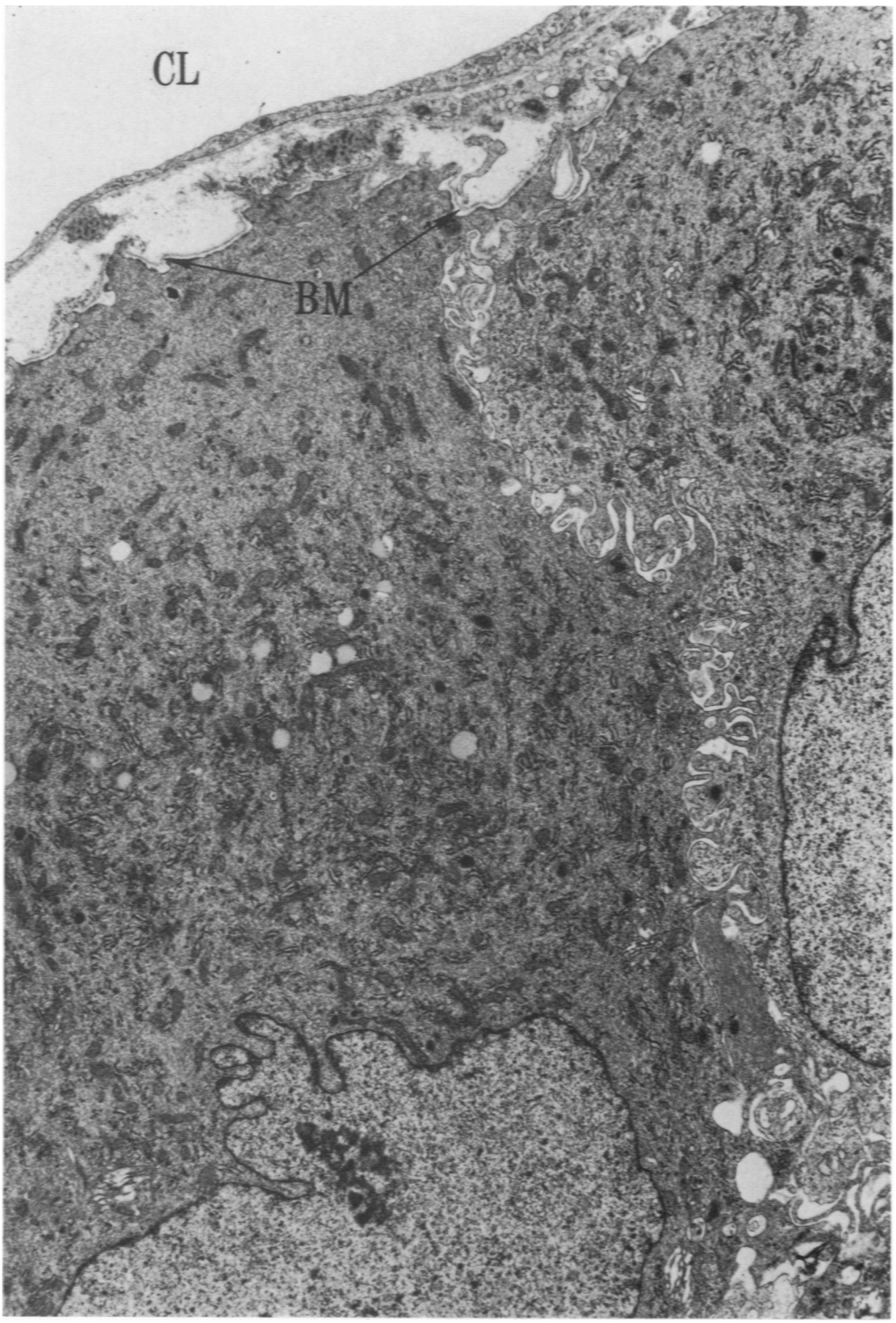

Figure 9—Two gemistocytic astrocytes adjacent to an endothelial cell lining a capillary lumen (*CL*). Basement membrane (*BM*) is present on the astrocytic cell surface at the endothelial interface but is absent between astrocytes. (Formaldehyde fixation, × 9690)

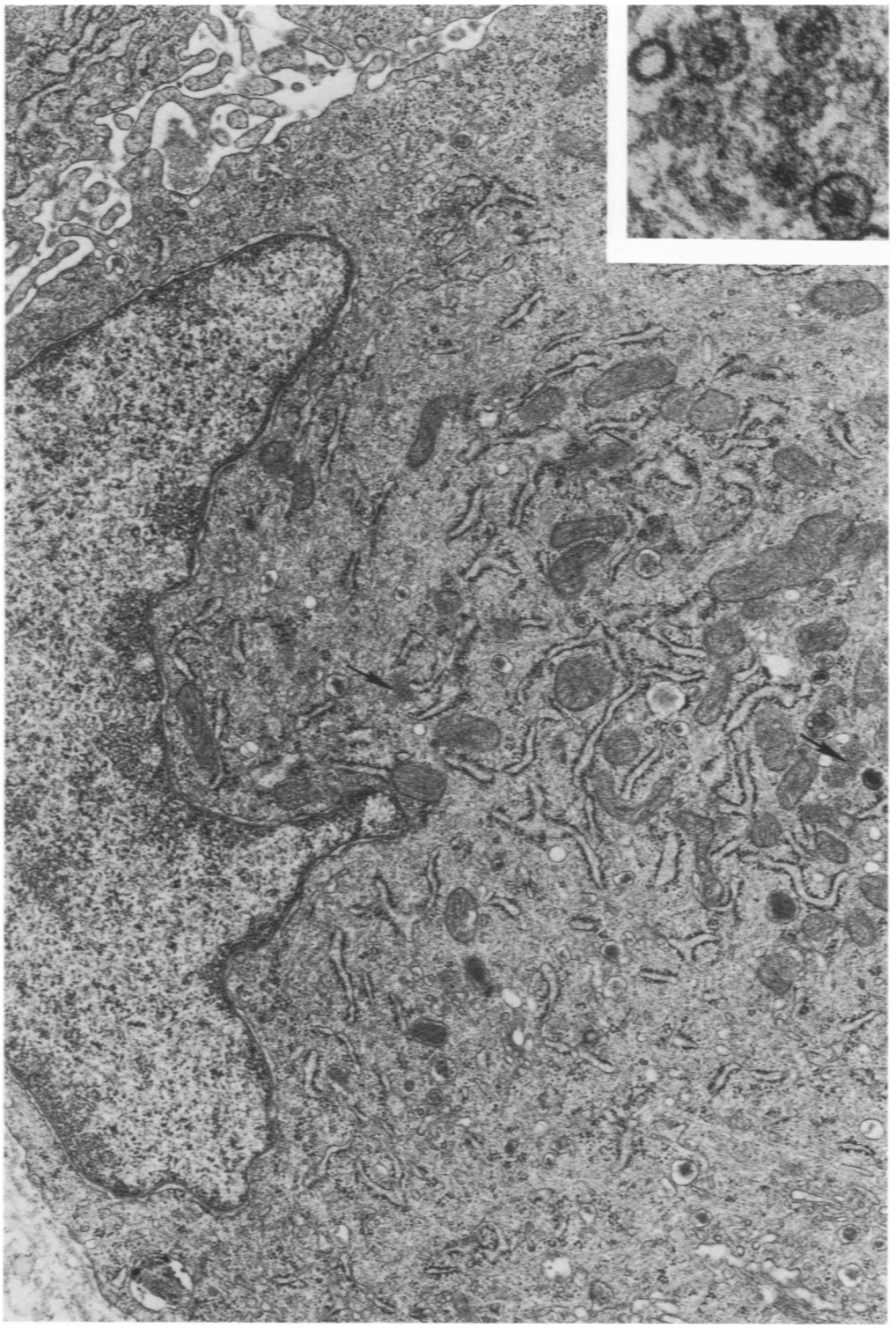

Figure 10—Detailed view of the perinuclear region of a gemistocytic astrocyte showing cytoplasmic organelles, 7- to 9-nm filaments, and R particles (*arrows*) (× 19,150). **Inset**—R-particles from another cell showing inner core and radiating spokes; note that some cores are hollow and others electron dense (Formaldehyde fixation, × 143,600).

Figure 11—Detail of gemistocytic astrocyte showing contiguity of amorphous lipid and cytosegresomes; note numerous Golgi profiles and invagination of nuclear membrane (Formaldehyde fixation, × 13,680).

Figure 12—Extreme invagination of nuclear membrane in a gemistocytic astrocyte (Formaldehyde fixation, × 6200).

Figure 13—Light micrograph of a 1-μ-thick section stained with toluidine blue showing invasion of chroid plexus epithelium (*CPE*) by gemistocytic astrocytes (Formaldehyde fixation, × 375).

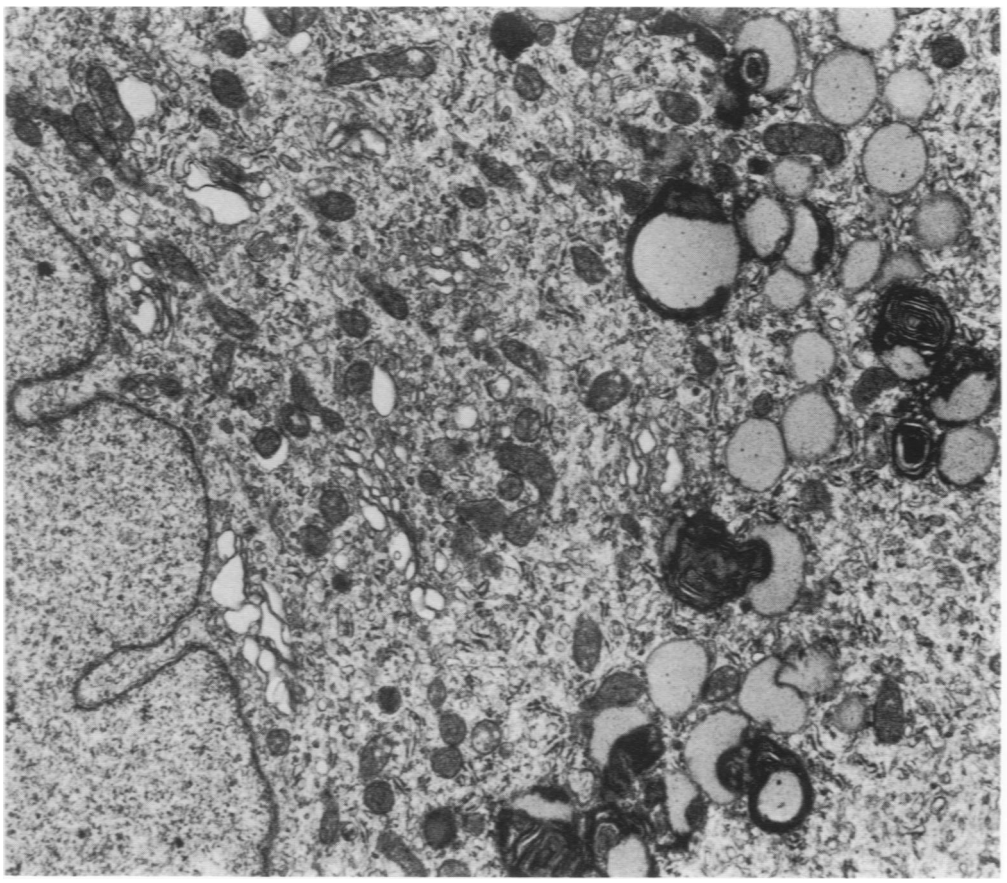

11

2

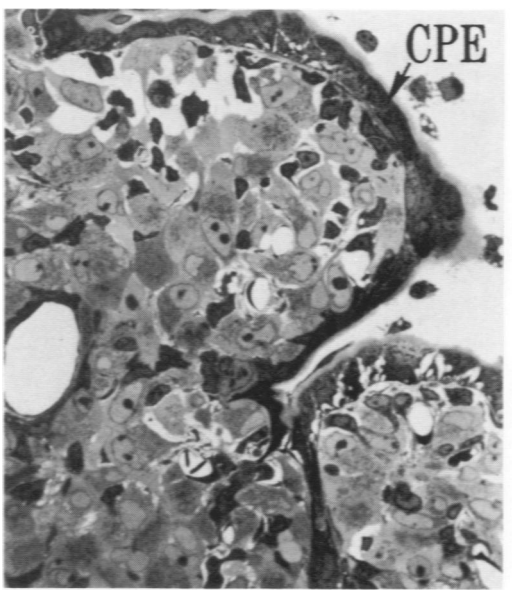

13

14

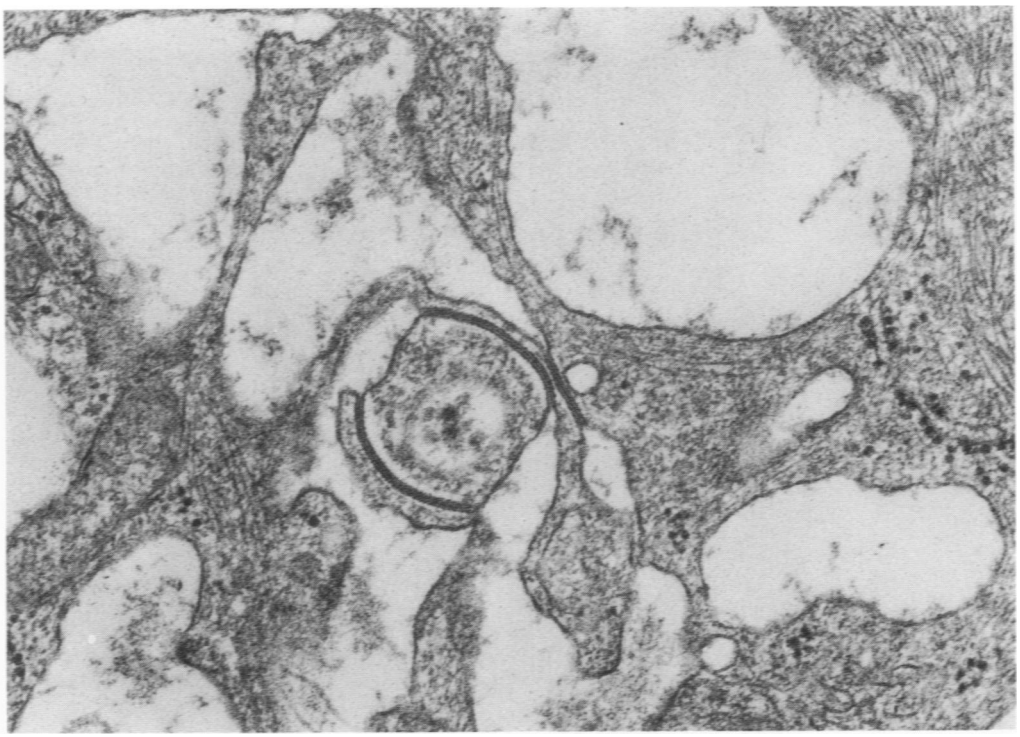

15

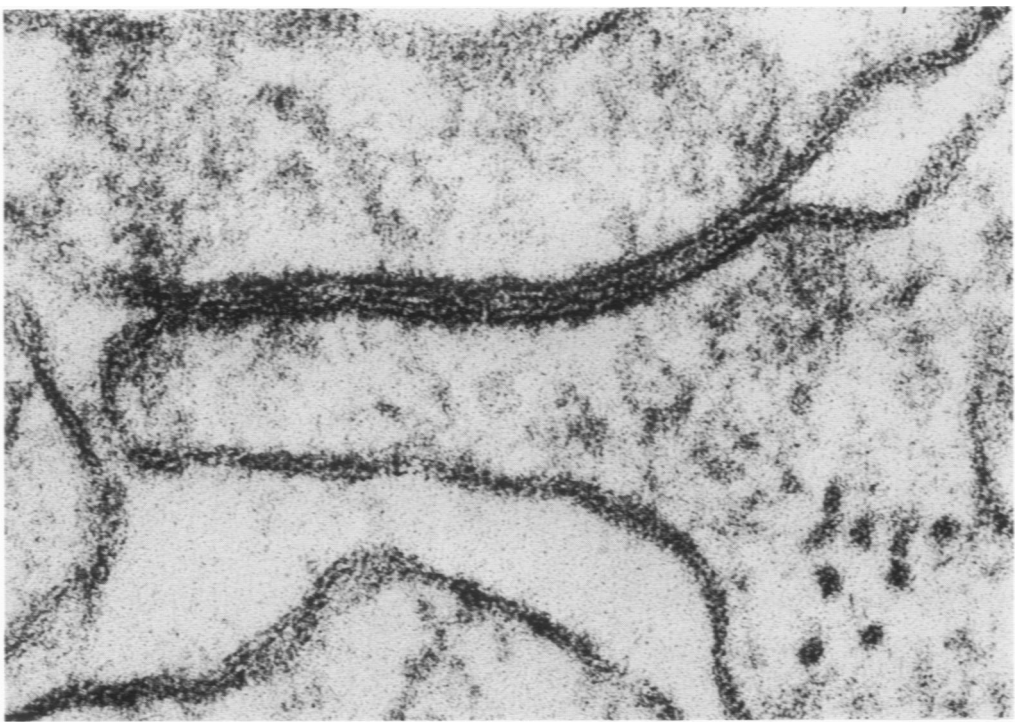

Figure 14—Gap junction between the processes of a cell intermediate in morphology between poorly differentiated and gemistocytic forms (Glutaraldehyde fixation, × 59,200). **Figure 15**—Gap junction between processes of pilocytic astrocytes showing 3- to 4-nm gap between outer leaflets of apposed cell membranes. Note end view of 7- to 9-nm intracellular filaments showing hollow core. (Formaldehyde fixation, × 205,428)

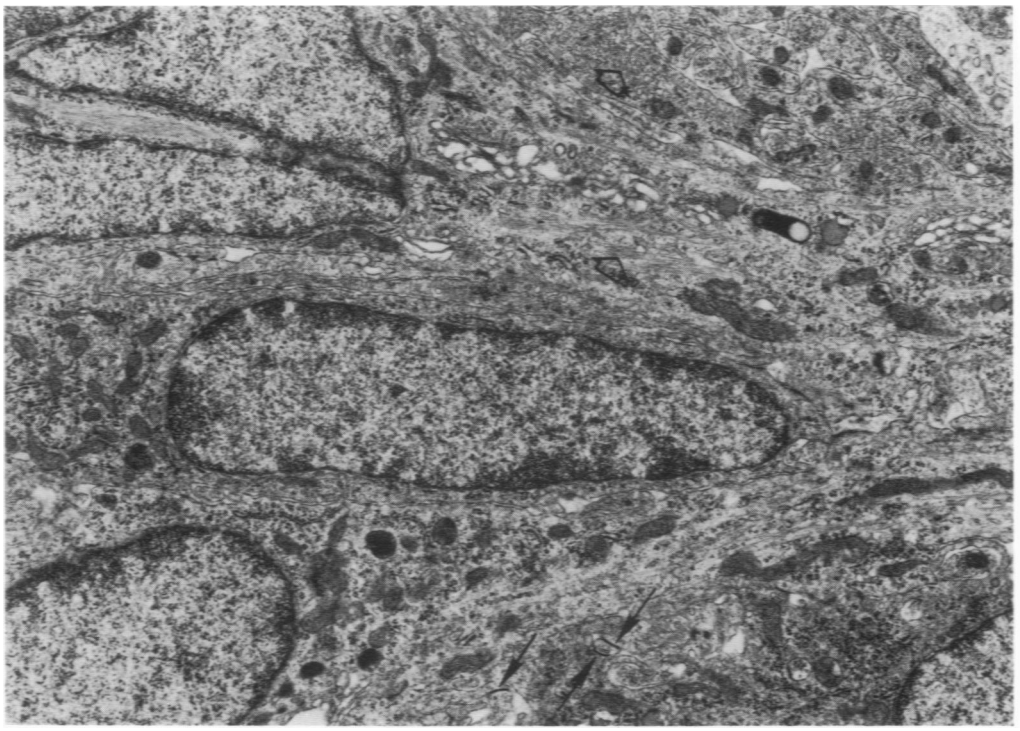

16

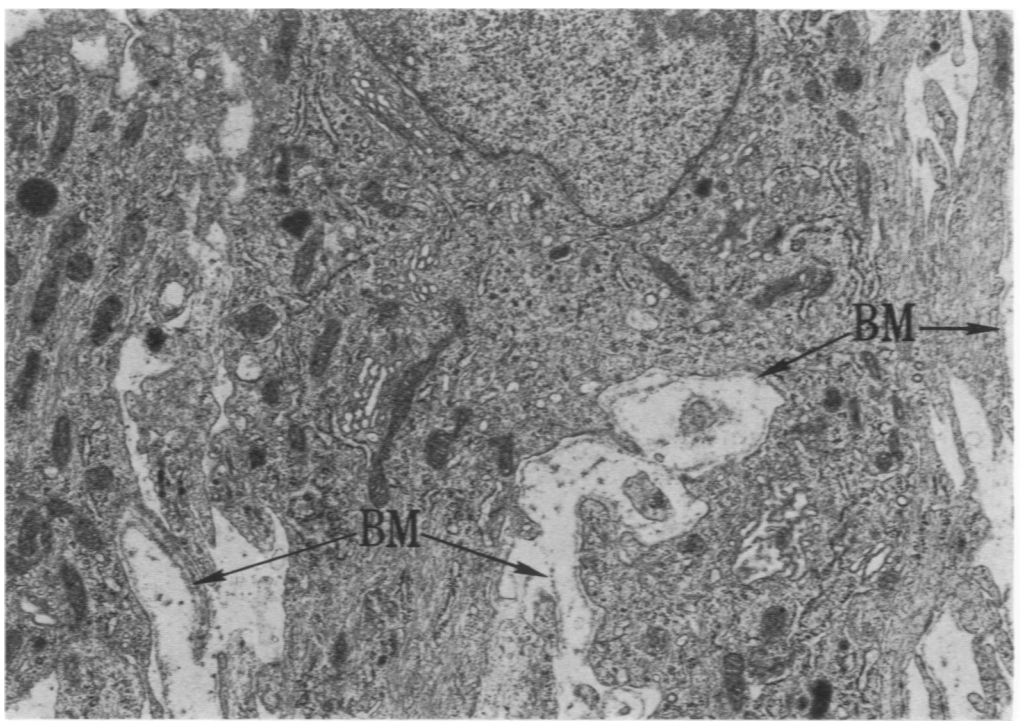

17

Figure 16—Spongioblast-like cells in a poorly differentiated astrocytoma. Note junctions (*solid arrows*) and filaments (*hollow arrows*) in longitudinal and end views. (Formaldehyde fixation, × 12,900) **Figure 17**—Neoplastic astrocytes in a pilocytic astrocytoma; basement membrane (*BM*) covers some but not all cell surfaces (Formaldehyde fixation, × 12,270).

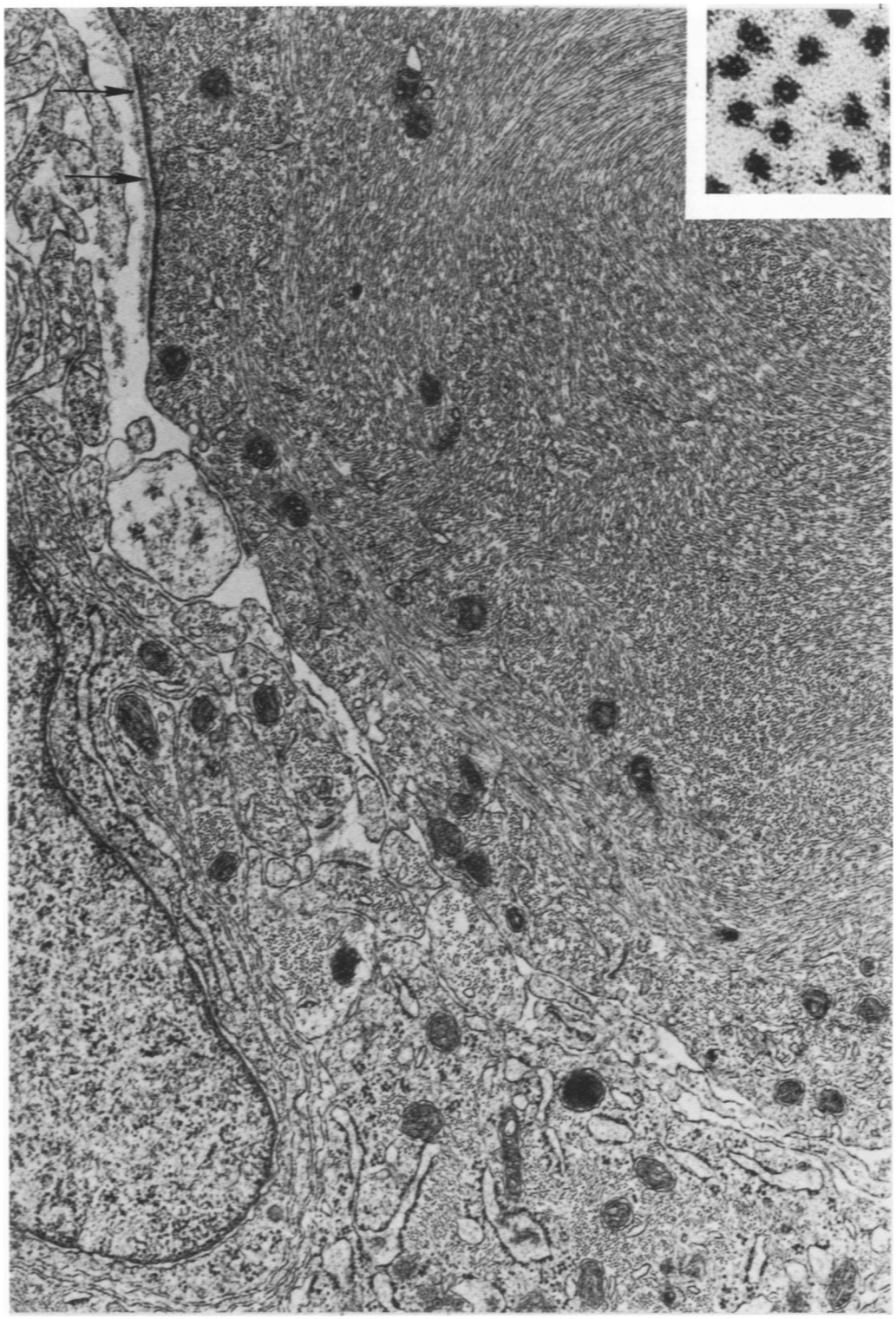

Figure 18—Marked glial fibrillogenesis in a pilocytic astrocytoma; note basement membrane (*arrows*) (× 28,720). **Inset**—End view of 7- to 9-nm filaments in large cell showing hollow core and suggestion of globular subunits in wall (Formaldehyde fixation, × 490,000).